Modeling of Wind Turbine Transformers for the Analysis of Resonant Overvoltages

Amir Hayati Soloot, Hans Kristian Høidalen and Bjørn Gustavsen

Abstract-- **Switching transients and earth fault in a wind farm collection grid are two transient phenomena which can lead to resonant overvoltages at the LV terminal of the wind turbine transformers as well as inside HV and LV windings. The aim of this paper is to analyze the potential of resonant overvoltage for various winding designs; disc, layer and pancake. In this way, the less vulnerable winding design can be recommended. For this aim, a 500 kVA transformer test object with the three aforementioned winding types has been designed and manufactured. Similar geometrical characteristics are used for all the three windings. By measuring the frequency response, the resonance frequencies can be found and the amplitude of transferred voltage at these frequencies can be compared. The windings are also modeled in this paper in detail based on analytical functions. This RLC ladder model is verified by the measurements.**

The measurements show that all winding designs have a resonance frequency around 800 kHz for the transferred voltage to LV terminal. Disc winding shows the lowest amplitude of the transferred overvoltages (6 p.u.). The layer winding, also has a resonance at 1.6 MHz with an even higher transferred overvoltage (80 p.u.). The frequency response of pancake winding has characteristics of both disc and layer windings. In spite of having the lowest transferred overvoltage peak, the disc winding have many additional resonance frequencies in the range of 100 kHz-1MHz. This could excite resonances in other parts of the winding. Consequently, pancake winding designs might be the most promising to minimize resonance situations.

***Keywords*: Wind turbine transformer, resonant overvoltages, winding design, analytical modeling, RLC ladder model.**

I. Introduction

MEDIUM voltage transformers with ratings in the range of 300kVA-8MVA have been installed in both onshore and offshore wind farms. The energization of each wind turbine may result in cable-transformer resonant transients. This phenomenon has been studied in traditional medium voltage transmission and distribution networks in [1]-[2]. The similar resonance condition can also happen in wind farms. The length of cables in wind turbines is in the range of 100-200 m. The quarter wave frequency of such cables can be in the vicinity of resonance frequencies of wind turbine transformers. Therefore, the energization may lead to resonant overvoltages on LV terminal of transformers and inside HV windings. These overvoltages have higher amplitude and rate of rise (du/dt) compared to other overvoltages. They can lead to insulation failures in transformers. In [3], the voltage distribution due to energization of a 10 kV-200 kVA reactor with disc winding is analyzed. It was observed that energizations with short rise time (<100ns) leads to the excitation of internal resonances. Resonant overvoltages can also occur due to earth fault in cables. In this case, they can be harmful for the power converters as well. Thus, the investigation of them is necessary [4] and appropriate protection devices such as Resistive-Capacitive (RC) filters are required [5]-[6].

The selection of less vulnerable winding design is a measure to prevent resonant overvoltages during wind turbine energizations. This means that knowing the cable lengths and their quarter wave frequency, a winding type can be chosen that does not have a resonance frequency in that vicinity. The aim of this paper is to compare frequency responses of three winding types; disc, layer and pancake. A 500 kVA transformer with the three aforementioned winding types has been designed and manufactured.

An analytical model is also developed and introduced in this paper. The model assists us to draw general conclusions about the various characteristics of the three winding designs and their potential for resonant overvoltages. In literature, two main high frequency transformer modeling techniques are introduced as Multi Transmission Line (MTL) model and ladder RLC [7]. In [8], results from MTL and RLC ladder models of windings are compared with frequency domain measurements. It is concluded that the RLC model can give adequate results for fast transients (up to 1 MHz). However, for very fast transients (above 1 MHz) MTL model provides better results. In this paper, RLC ladder model is developed, since the maximum range of the quarter wave frequency of wind turbine cables are about 1 MHz.

In section II, the transformer test object and the setup for frequency response analysis are outlined. Section III describes the transformer model. In section IV, the results of the analytical models for the different windings are compared. The characteristics of the three windings are also discussed. Section V discusses the challenges of transformer modeling.

II. Test Setup

Fig. 1 shows the layout of the special 11/0.24 kV 500 kVA

This work was supported by the Norwegian Research Center for Offshore Wind Farm(NOWITECH)-Work package (4).

A. H. Soloot and H. K. Høidalen are with the Department of Electrical Power Engineering, Norwegian University of Science and Technology (NTNU), Trondheim N-7491, Norway (e-mail: amir.h.soloot@elkraft.ntnu.no, e-mail: hans.hoidalen@elkraft.ntnu.no).

B. Gustavsen is with SINTEF Energy Research, Trondheim N-7465, Norway (e-mail: bjorn.gustavsen@sintef.no).

Paper submitted to the International Conference on Power Systems Transients (IPST2013) in Vancouver, Canada July 18-20, 2013.

transformer which is designed and produced to enable comparison of the frequency response of the three different winding designs. The core and the windings are fully paper insulated and out of tank during the measurements. The LV and HV neutrals are grounded together and connected to the core with 2 cm wide braided aluminum wire.

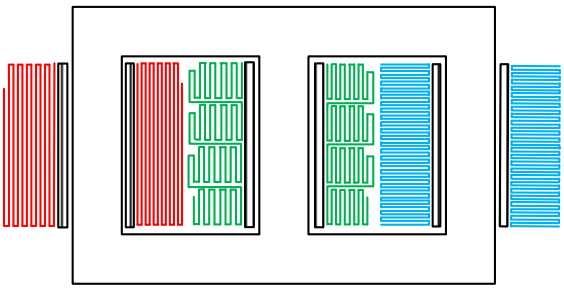

Fig. 1. The layout of the manufactured 500 kVA transformer

As shown in Fig. 1, the transformer consists of a layer winding on the left limb, a pancake winding on the middle and a disc winding on the right limb. To compare the frequency response of the windings, design parameters are kept as identical as possible:

- The number of turns in HV and LV windings and rated voltage ratio are the same for the winding designs.
- The winding frame, i.e. axial winding height and radial width, is approximately the same for the windings.
- The layer winding has aluminum wire and the others have copper wires. The conductor cross section is such that the DC resistance of the windings becomes similar.
- LV windings are all aluminum foil with the same geometrical designs and insulation materials.

The frequency responses of transferred voltages to LV terminals is measured from 1 kHz to 10MHz with Agilent network analyzer E5061B and normal oscilloscope probes with x10 attenuation. For measuring the input impedance of HV and LV windings, the current probe FLUKE PM6306 is used, which has low and acceptable error (<10%) in frequency range 1kHz-1MHz. Therefore, the results for input impedance will be shown in this frequency range in the next section.

III. Transformer Model

The three winding types; disc, pancake and layer windings and the LV foil winding are represented by RLC ladder model in this paper. This requires calculation of inductance, capacitance and resistance matrices to obtain the input impedance of HV and LV windings and consequently the transferred voltage from HV to LV. The accuracy of the model mainly depends on the level of discretization chosen for the windings. High discretization increases the calculation time. The procedure for the calculation of RLC parameters is explained here for layer winding. It is generally similar for the other windings with only topological adjustments.

Let us consider *nu* number of units in each layer of HV layer winding. *nH* is the number of HV layers and therefore *nu*×*nH* is the total number of units. Besides, the LV foil winding has *nL* layers, and we take each layer as one unit. The total order of *R*, *L*, *C* and *G* matrices becomes *m*=*nL*+*nu*×*nH*.

Performing the Kirchhoff's Voltage Law (KVL) and Kirchhoff's Current Law (KCL) for all units results in (1) and (2), respectively. In Appendix, KCL and KVL for an arbitrary unit, *i*, is performed.

$$[A]_{m\times m}[V]_{m\times 1} = ([R]_{m\times m} + j2\pi f[L]_{m\times m})[I_b]_{m\times 1} \quad (1)$$

$$[I]_{m\times 1} - [A]^t_{m\times m}[I_b]_{m\times 1} = ([G]_{m\times m} + j2\pi f[C]_{m\times m})[V]_{m\times 1} \quad (2)$$

Matrices V, I and I_b representing nodal voltages, injected nodal currents, the currents of inductive branches, respectively. A is a connectivity matrix describing the topology and linking branches and nodal quantities. The diagonal elements in A matrix are equal to 1 and sub-diagonal elements are equal to -1 and the rest is zero. Exceptionally, the first row and the row number nL+1, which are for first units in LV and HV winding respectively, have only the diagonal element, since the other nodes of these units are grounded.

The nodal admittance matrix Y can be calculated by reforming (1) to obtain I_b based on V and inserting this in (2). This gives (3).

$$[I] = [Y][V] \quad (3)$$
$$[Y] = [G] + j2\pi f[C] + [A]^t([R] + j2\pi f[L])^{-1}[A]$$

Since all of the *R*, *L*, *C* and *G* matrices are symmetrical, the admittance matrix also becomes symmetrical. To obtain the equation for the transferred voltage to LV, impedance matrix, *Z*, should be calculated from (3) by inverting *Y*. Since only the last element of the *I* vector is none-zero due to the connection of last unit to the HV terminal, the last column of *Z* multiplies with the terminal current, I_m and gives the nodal voltage in (4). Therefore, transferred voltage to LV terminal is according to (5).

$$[Z(:,m)]I_m = [V] \quad (4)$$

$$V_{LV}/V_{HV} = Z(nL,m)/Z(m,m) \quad (5)$$

In the following subsections, the process for calculation of the *R*, *L*, *C* and *G* matrices are explained.

A. Calculation of R and L matrices

The analytical method [9]-[10] for computing the self and mutual impedance is based on the equations (12)-(15) in the Appendix. In addition, the internal conductor resistance is added to diagonal elements of *R* matrix, since Wilcox formulas only consider the core effect on the resistance matrix. In this paper, an analytical equation for the consideration of skin and proximity effects is applied for the calculation of internal conductor resistances [11] in both LV and HV winding:

$$R_{LV}(n) = Re\{\frac{\pi D(n)\gamma}{2\sigma h}[\coth(\gamma w)\,(2n^2 - 2n + 1) - \frac{(2n(n-1))}{\sinh(\gamma w)}]\} \quad (6)$$

$$\gamma = \frac{1+i}{\delta}\sqrt{\eta} = (1+i)(\sqrt{\pi\mu_0\sigma f})\sqrt{\frac{h}{p}}$$

In (6), the layer number is symbolized with n. The diameter of n^{th} layer is $D(n)$. The conductor height and width are h and w, respectively. The skin depth in each conductor is shown with δ and is related to its conductivity, σ, frequency, f, and its permeability, $\mu=\mu_0$. The conductor height plus its insulation height is p. The ratio of h to p is called porosity factor, η. For LV foil winding, η is one with good approximation. For HV pancake and layer winding, $0.9< \eta<1$. While for disc winding, it is $0.7< \eta<0.9$. Since, the inter disc insulations increase the insulation height.

B. Calculation of C matrix

The diagonal elements of C matrix are the sum of capacitances connected to each unit. While the off diagonal elements are all negative and equal to the capacitance between the unit which has the row number and other units. It is obvious that there are many zero elements in C matrix, since each unit has just capacitive coupling with four other units, e.g. in layer winding the two adjacent units in the same layer, one unit in layer before and one unit in layer after. The capacitance between adjacent units is calculated based on (7),

$$C_{ij} = \varepsilon_0\varepsilon_r\frac{\pi D(T+t)}{t} \quad (7)$$

The permittivity of vacuum and the relative permittivity of the insulation between units are shown with ε_0 and ε_r, respectively. D is the average diameter of two adjacent units. T is unit height if units are in adjacent layers or unit thickness if they are next to each other in one layer. The insulation thickness is shown with t. The fringing effect, which is the increment of the capacitances due to curvature of electric field lines in the edge of conductor, is considered by adding t to w [12].

C. Calculation of G matrix

The conductivity matrix, G, is calculated based on conductance of insulations between units. The insulation conductance is related to its capacitance and dissipation factor ($tan\delta$).

$$G_{ij} = 2\pi f tan\delta C_{ij} \quad (8)$$

Similar to C matrix, the diagonal elements on G matrix are the sum of conductance connected to each unit. While the off diagonal elements are all negative and equal to the conductance between the unit which has the row number and other units. It should be mentioned that $tan\delta$ in (8) is also frequency, moisture and temperature dependent and has important effect for high frequency transformer model above 100 kHz [13]. Therefore, accurate modeling really necessitates obtaining the frequency dependency of all insulations; the ones between LV foils, HV units, between LV and HV, LV to ground and HV to ground. In this paper, we used an approximated equation, (9), for all the insulation dissipation factors [14],

$$\tan(\delta) = (1{,}082 \times 10^{-8}).2\pi f + 5{,}0 \times 10^{-3} \quad (9)$$

IV. Model Verification and Winding Comparison

The results of modeling the three windings are brought in this section and compared with measurements. Besides, considerations for the energization of wind farms are given.

A. Layer winding

In Figs. 2 and 3, the input impedance of HV layer winding and the LV foil winding are shown. It can be observed that the calculations follow the decreasing trend of the measurement for Layer winding in both HV and LV windings.

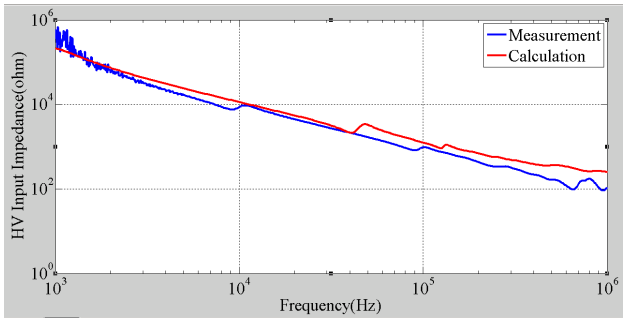

Fig. 2. HV input impedance for layer winding

The shortcoming of the model is that the second resonance frequency (10kHz) is not represented. Besides, the amplitude of model response for LV winding (Fig. 3) at f=1 MHz is higher than measurement.

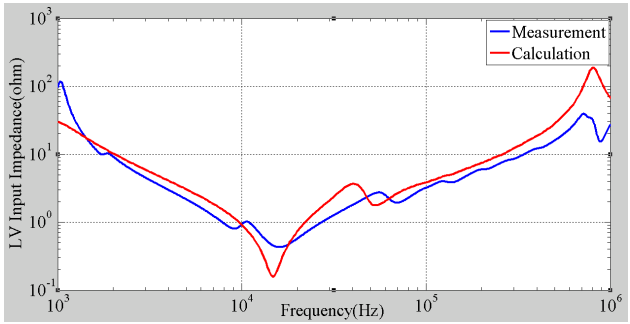

Fig. 3. LV input impedance for layer winding

The induced voltage on the LV terminal calculated by (5) is compared with measurements in Fig. 4. The frequency range is now extended to 10 MHz, since the voltage probes are accurate also above 1MHz. Although quarter wave frequency of wind park feeder cables rarely can be in this range, close-up ground faults can give oscillations with such high frequencies.

This also gives an opportunity to test the analytical model at higher frequencies.

As it can be seen in Fig. 4, the model results are in good agreement with measurements for f<1MHz. But, for f>1MHz, it only follows the decreasing trend of the measurements. The dominant resonance frequency in 1.6 MHz is not well represented. This will be discussed in detail in discussion section.

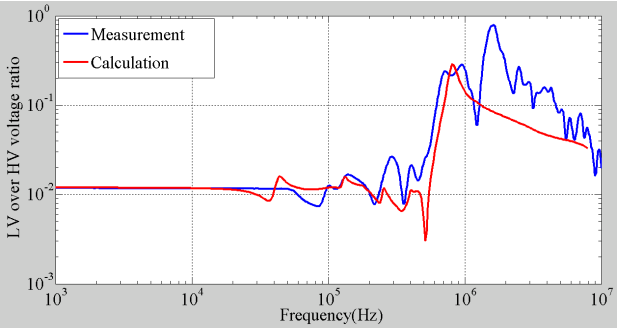

Fig. 4. Transferred voltage from HV to LV for layer winding

B. Disc winding

In Figs. 5 and 6, the input impedance of HV disc winding and its LV foil winding are shown. One weakness for the calculations for the disc winding is the shift in the LV input impedance for f>20kHz.

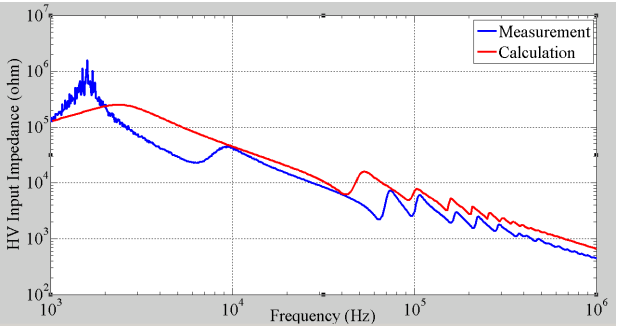

Fig. 5. HV input impedance for disc winding

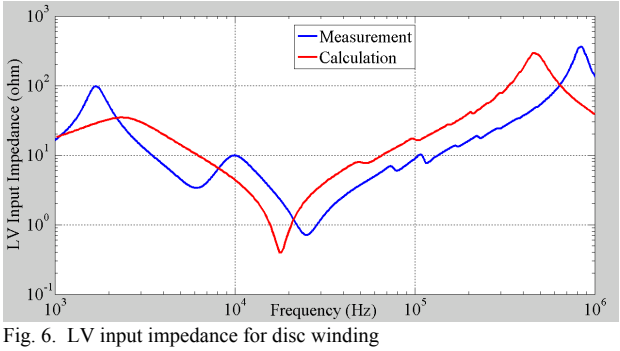

Fig. 6. LV input impedance for disc winding

The induced voltage to LV terminal is compared with measurements in Fig. 7 for the disc winding. The model response follows the trend of measurement and represents some of the resonance frequencies and especially the dominant one. Comparing Fig. 7 and Fig. 4, it can be seen that the amplitude of transferred voltage to LV at 800 kHz, which is the common resonance frequency and the dominant one for disc winding, is much lower for the disc winding. Despite that, the disc winding has many resonance frequencies around 100 kHz, while layer winding has most of its resonance frequencies above 1MHz. The resonance frequencies of disc winding are in the range of quarter wave frequency of typical wind turbines. They can be amplified inside HV or at LV windings. Therefore, there can be high potential of internal resonant overvoltages.

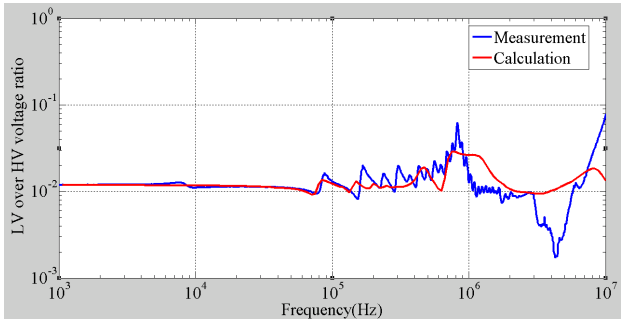

Fig. 7. Transferred voltage from HV to LV for disc winding

C. Pancake winding

In Figs. 8 and 9, the input impedance of HV pancake winding and its LV foil winding are illustrated. Compared to disc winding, the frequency shift in the LV model response is smaller but still present.

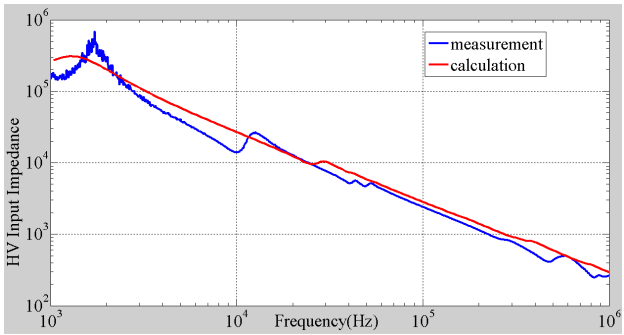

Fig. 8. HV input impedance for pancake winding

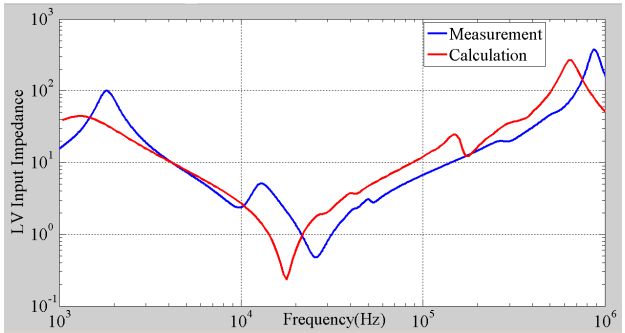

Fig. 9. LV input impedance for pancake winding.

The induced voltage to the LV terminal is compared with measurements in Fig. 10. It seems that, the model results can not represent the amplitude of measurement near 800 kHz. Comparing measurement results for the transferred voltage to

LV for the three windings in Fig. 11, the trend of the frequency response around 800 kHz for the pancake winding is similar to the disc winding, while the amplitude of the transferred voltage is in the range of the layer winding.

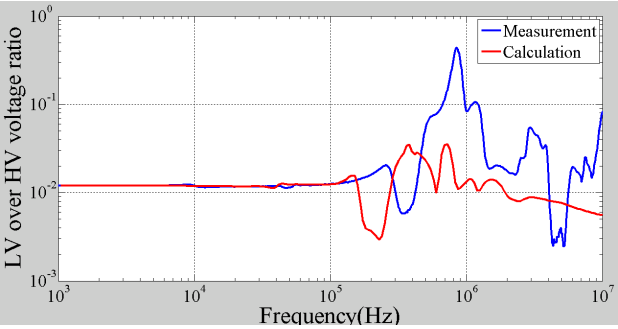

Fig. 10. Transferred voltage from HV to LV for pancake winding

It can be concluded that if the quarter wave frequency of feeder cables is lower than 800 kHz, pancake and layer windings may be the less vulnerable winding for internal resonant overvoltages. Meanwhile, pancake winding has the advantage of repair easiness. For example, the pancake winding here has four coils. If any internal insulation failure happens in any coils, it can be easily replaced. This feature is prominent for offshore wind farms, where long distance from shore and accessibility challenges requires maintenance-free or easy repairing components.

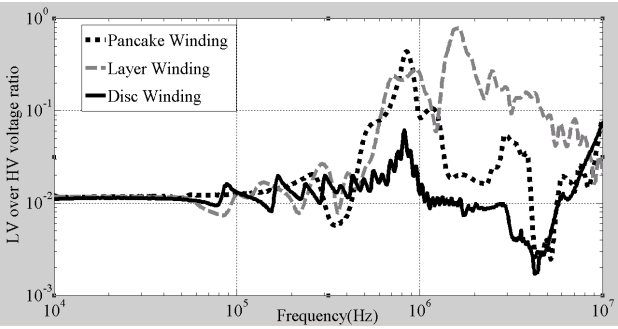

Fig. 11. Measured transferred voltage from HV to LV for the three windings

V. Discussion

The white box models; RLC ladder model and MTL model require precise geometrical data and material property of the transformer under study. In this work, we designed and produced this 500 kVA transformer. Therefore, detailed geometrical design data are available. Most of coil, core, and insulation material property are also known. However, the detailed frequency dependency of the dissipation factors (tanδ) of all transformer insulators, which is needed for accurate modeling, especially f>1 MHz is not available. Therefore, equation (9) from literature is just included for all transformer insulations.

The next issue to be discussed is the analytical calculation of internal conductor resistance, which is one part of self-resistance. The other part is the self-resistance due to the core and is calculated by Wilcox formula. Fig. 12 shows the total self-resistance of LV foil associated with disc winding according to the proposed model. The black solid line represents self-resistance due to core skin effect. The dashed line shows the internal conductor resistance based on (6). The dashed-dotted line is the internal conductor resistance only due to skin effect [15].

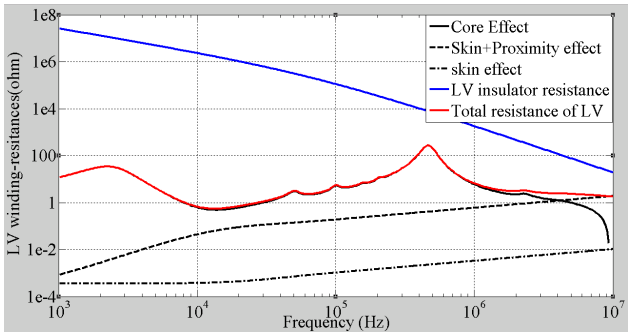

Fig. 12. The comparison of different resistances in LV winding with total resistance.

It can be found that total resistance is dominantly affected by proximity effect for f>4MHz. Ignoring the proximity effect in the model and including just skin effect by the analytical formula in [15] leads to resonance frequencies, around 100 kHz, with quite high amplitudes for the transferred voltage to LV in layer winding (see Fig. 13). The internal conductor resistance becomes two orders of magnitude lower for 10 kHz<f<1MHz by ignoring proximity. The calculation results for transferred voltage in this case has poor agreement with measurement for 50 kHz<f<500kHz.

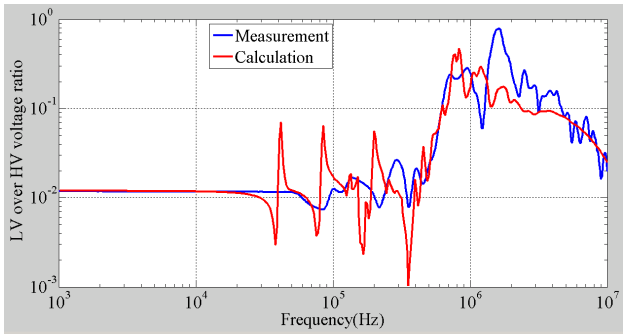

Fig. 13. Transferred voltage from HV to LV for layer winding. Proximity effect ignored in the calculations.

VI. Conclusions

In this paper, the frequency response of layer, pancake and disc winding types are studied with focus on resonant overvoltages in wind turbines. A special 500 kVA transformer with three different winding designs is produced and used as test object. The frequency responses of input HV impedance, input LV impedance and transferred voltage to LV are measured. Analytical RLC model of the windings is proposed in this paper and compared with measurements. The calculations show that the following characteristics of the windings are represented in good qualitative agreement with

measurements:

1- The general trend of the frequency response for the windings, i.e. the range of amplitude for input impedance and voltage ratio
2- The decreasing trend of HV input impedance.
3- The resonance frequencies of HV and LV input impedances in the range of 10kHz-1MHz.
4- The dominant resonance frequency of transferred voltage to LV for disc and pancake winding (800 kHz). This frequency is also critical for layer winding.

The shortcomings of the model can also be listed as:

1- The second resonance frequency (=10kHz) of the input impedance of the HV and LV windings is not represented. It can be due to flux linkage of other windings via core.
2- There is a frequency shift between impedance measurements and calculations.
3- The model cannot represent the voltage ratio measurements for f>1MHz. It can be due to inaccuracy in measurements due to effect of leads, inaccuracies in the proximity effect or dissipation factors (tanδ) formulas.

In fact, the qualitatively good agreement of the calculation model assists us to study the internal overvoltages in future work. It can assist wind turbine operators to energize wind turbines with lower risk of resonant overvoltage. The least vulnerable winding design seems in this case to be the pancake winding. Its modular design makes it also easier to repair compared to the two other winding types.

VII. Appendix

A. KCL and KVL for an arbitrary unit

Figure 14 shows an arbitrary unit, *i*, in HV winding and its adjacent unit. Performing KVL in this unit gives,

$$V_i - V_{i-1} = z_{i,i} I_b(i) + z_{i,i-1} I_b(i-1) + z_{i,i+1} I_b(i+1) + z_{i,m} I_b(m) + z_{i,n} I_b(n) + \cdots \quad (10)$$

Mutual impedance of the unit *i* with other units is calculated by means of (12). Self-impedance, $z_{i,i}$, is calculated by adding the internal resistance (6) to (12). Writing KVL for all units in LV and HV result in (1).

To perform KCL, an injected nodal current, *I*, is connected to node *i* (see Fig. 14). The sum of all branch currents is equal to *I*.

$$\begin{aligned} I = {} & I_b(i) - I_b(i+1) + \\ & \big(G(i,i-1) + j2\pi f C(i,i-1)\big)\big(V(i) - V(i-1)\big) + \\ & \big(G(i,i+1) + j2\pi f C(i,i+1)\big)\big(V(i) - V(i+1)\big) + \\ & \big(G(i,m) + j2\pi f C(i,m)\big)\big(V(i) - V(m)\big) + \\ & \big(G(i,n) + j2\pi f C(i,n)\big)\big(V(i) - V(n)\big) \end{aligned} \quad (11)$$

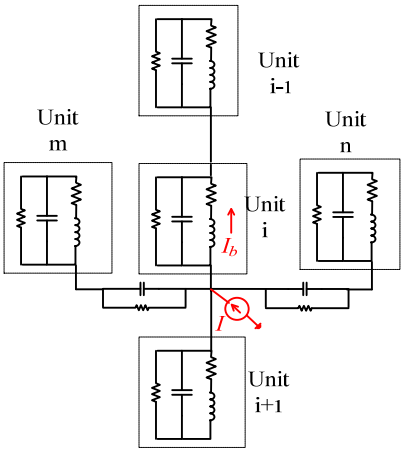

Fig. 14. The layout of unit *i*, an arbitrary unit in HV windings

Writing KCL for all units in LV and HV and doing simple mathematical manipulation result in (2). Besides, equation (11) shows that the summation of all adjacent capacitors of unit *i* come into the diagonal element of *C* matrix. Since they are all multiplied to *V(i)*.

B. Computation of the self and mutual impedance

Figure 15 shows two arbitrary units around the core. Assuming the core as a solid magnetic material with μ_z in the axial direction, μ_r in the radial direction and an isotropic resistivity ρ, equations (12)-(15) describe the mutual impedance between these two units [9].

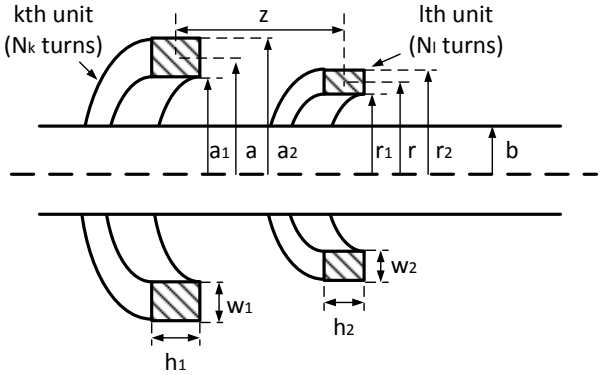

Fig. 15. Dimensions of two arbitrary units for the calculation of self and mutual impedances.

$$z_{kl} = sL_{kl} + z_{1(kl)} + z_{2(kl)} \quad (12)$$

$$L_{kl} \cong \mu_0 N_k N_l \sqrt{ra}\,\frac{2}{p}\left[\left(1 - \frac{p^2}{2}\right)K(p) - E(p)\right] \quad (13)$$

$$z_{1(kl)} = sN_k N_l \frac{\pi b^2}{\lambda}\left\{\frac{2\mu_z I_1(mb)}{mbI_0(mb)} - \mu_0\right\} \quad (14)$$

$$z_{2(kl)} = sN_kN_l\frac{\pi}{\lambda}\left\{\frac{4}{h_1h_2w_1w_2}\sum_{n=1}^{N}P_1(\beta_n a_1,\beta_n a_2)\right.$$
$$\times P_1(\beta_n r_1,\beta_n r_2)Q_1(\beta_n h_1,\beta_n h_2) \quad (15)$$
$$\left.\times\frac{I_1(\beta_n b)F_1(\beta_n b)}{K_1(\beta_n b)}\cos(\beta_n z)\right\}$$

s is the Laplace transform operator in (12). In (13), *K(p)* and *E(p)* are complete elliptic integrals of the first and second kinds respectively, and

$$p = \sqrt{\frac{4ar}{z^2+(a+r)^2}} \quad (16)$$

The dimensions *a*, *r* and *z* are specified in Fig. 15. In (14), the core skin effect parameter, *m*, is equal to,

$$m = \sqrt{\frac{s\mu_z}{\rho}} \quad (17)$$

In (15), β_n=2πn/λ, where λ is the length of the magnetic circuit. I_0, I_1,K_0 and K_1 are modified Bessel functions. The functions *P*, *Q*, and F, are defined in (18)-(21).

$$P_1(x,y) = \frac{1}{\beta_n^2}[p_1(x)-p_1(y)] \quad (18)$$

$$Q_1(\mathrm{x},\mathrm{y}) = \frac{2}{\beta_n^2}\left[\cos(\frac{x-y}{2})-\cos(\frac{x+y}{2})\right] \quad (19)$$

$$F_1(\beta_n \mathrm{b}) = \mu_0\left\{\frac{\mu_z.f(\beta_n \mathrm{b})-\mu_0.f(\Gamma_n \mathrm{b})}{\mu_z.g(\beta_n \mathrm{b})+\mu_0.f(\Gamma_n \mathrm{b})}\right\} \quad (20)$$

$$\Gamma_n = \sqrt{\frac{\mu_z}{\mu_r}\beta_n^2+\frac{s\mu_z}{\rho'}} \quad (21)$$

In (21), $\rho'=\gamma.|s|$ and γ is defined as fundamental core parameter related to leakage flux and is in the range of 10^{-10}-10^{-8} [9]. The functions *f*, *g* and p_1 are defined by

$$f(\xi) = \xi\frac{I_0(\xi)}{I_1(\xi)} \quad (22)$$

$$g(\xi) = \xi\frac{K_0(\xi)}{K_1(\xi)} \quad (23)$$

$$p_1(\alpha) = \frac{\pi\alpha}{2}[K_1(\alpha)L_0(\alpha)+K_0(\alpha)L_1(\alpha)] \quad (24)$$

In (24), $L_k(\alpha)$ is the modified Struve function,

$$L_k(\alpha) = \sum_{n=0}^{\infty}\frac{(0.5\alpha)^{k+2n+1}}{[n+0.5]![k+n+0.5]!} \quad (25)$$

It should be mentioned that for self-impedance calculation (Z_{kk}), *z* should be set to zero in (15) and *z=0.2235(h+w)* in (16) where *h* and *w* are height and width of the coil cross section.

VIII. Acknowledgment

Authors greatly appreciate Norwegian Research Center for Offshore Wind Technology (NOWITECH) which is sources of funding. They are also thankful of Møre Trafo Co. for their assistance in manufacturing the 500 kVA transformer test object.

IX. References

[1] B. Gustavsen, "Study of transformer resonant overvoltages caused by cable-transformer high frequency interaction," *IEEE transaction on Power Delivery*, Vol. 25, No. 2, pp. 770-779, April 2010.

[2] B. Gustavsen, A. P. Brede, and J. O. Tande, "Multivariate analysis of transformer resonance overvoltages in power stations," *IEEE transaction on Power Delivery*, vol. 26, no. 4, pp. 2563–2572, 2011.

[3] T. Abdulahovic:" Analysis of High-Frequency Electrical Transients in Offshore Wind Parks," Ph.D. dissertation, Dept. Energy and Environment, division of electric power eng., Göteborg : Chalmers University of Technology, 2011.

[4] A. H. Soloot, H. Kr. Hoidalen, B. Gustavsen, " Frequency domain investigation of switching transients in offshore wind farms", in proc. of IEEE Powertech conference, pp. 1-5, June 2011.

[5] A. H. Soloot, H. Kr. Hoidalen, B. Gustavsen, " A Study of switching Overvoltages in Offshore Wind Farm", in *proc. 2011 17th International Symposium on High Voltage Engineering*, paper B-30.

[6] A. H. Soloot, H. Kr. Hoidalen, B. Gustavsen, " The Assessment of Overvoltage Protection Within Energization of Offshore Wind Farms," *Energy Procedia*, vol. 24, pp. 151-158, 2012.

[7] J. A. Martinez-Velasco, *Power System Transients: Parameter Determination,* New York: CRC press-Taylor and Francis group, 2010, p. 222.

[8] S.M.H. Hosseini, M. Vakilian, and G.B. Gharehpetian, "Comparison of transformer detailed models for fast and very fast transient studies", *IEEE Transactions on Power Delivery*, vol. 23, no. 2, pp. 733–741, Apr. 2008.

[9] D. J. Wilcox, W. G. Hurley, and M. Conlon, "Calculation of self and mutual impedances between sections of transformer windings," *Proc. IEE. C*, vol. 136, no. 5, pp. 308–314, Sep. 1989.

[10] D. J. Wilcox, M. Conlon and W. G. Hurley, "Calculation of self and mutual impedances for coils on ferromagnetic cores", *IEE Proc. A.* ,vol. 135, no. 7, pp . 470-476,1988.

[11] M. K. Kazimierczuk, *High Frequency Magnetic Component,* West Sussex: Wiley, 2009, p. 186.

[12] S.V.Kulkarni, S.A.Khaparde, *TransformerEngineering: Design and Practice,* New York: Marcel Dekker, 2004, p. 286.

[13] E. Bjerkan, "High frequency modeling of power transformers-Stresses and Diagnostics," Ph.D. dissertation, Dept. Elc. Power. Eng., Norwegian Univ. of Science and Technology, Trondheim, 2005.

[14] E. Rahimpour, "Hochfrequente Modellierung von Transformatoren zur Berechnung der Übertragungsfunktion", Dissertation, University of Stuttgart, 2001.

[15] J. Lammeraner and M. Stafl, *Eddy Currents*, London: Iliffe books LTD., 1966, p. 21.